Chemistry–A European Journal
Research Article
doi.org/10.1002/chem.202203498
Chemistry Europe
European Chemical Societies Publishing
www.chemeurj.org

Synthesis and Single-Electron Oxidation of Bulky Bis(*m*-terphenyl)chalcogenides: The Quest for Kinetically Stabilized Radical Cations

Daniel Duvinage,[a] Farzin Mostaghimi,[a] Mattis Damrath,[a] Julian Spils,[a] Pascal Komorr,[a] Danila S. Odintsov,[b] Matvey Fedin,[c] Leonid A. Shundrin,*[b] Stefan Mebs,*[d] and Jens Beckmann*[a]

In memory of Professor Robert West.

Abstract: Sterically encumbered bis(*m*-terphenyl)chalcogenides, (2,6-$Mes_2C_6H_3)_2E$ (E = S, Se, Te) were obtained by the reaction of the chalcogen tetrafluorides, EF_4, with three equivalents of *m*-terphenyl lithium, 2,6-$Mes_2C_6H_3Li$. The single-electron oxidation of (2,6-$Mes_2C_6H_3)_2Te$ using XeF_2/$K[B(C_6F_5)_4]$ afforded the radical cation $[(2,6\text{-}Mes_2C_6H_3)_2Te][B(C_6F_5)_4]$ that was isolated and fully characterized. The electrochemical oxidation of the lighter homologs (2,6-$Mes_2C_6H_3)_2E$ (E = S, Se) was irreversible and impaired by rapid decomposition.

Introduction

Main group element centered radicals have received tremendous interest ever since Gomberg's seminal discovery of the trityl radical.[1,2] Amongst those, sulfur-based radicals play a pivotal role.[3–6] Diorgano sulfide radical cations, $[R_2S]^{\bullet+}$ (R = alkyl, aryl), generated from their neutral parents, R_2S, by chemical one-electron oxidation, photolysis in the presence of a sensitizer or gamma radiolysis are only short-lived.[7] In the absence of other fragmentation pathways, radical cations, $[R_2S]^{\bullet+}$, undergo complexation with their neutral parents, R_2S, giving rise to dinuclear radical cations, $[R_2SSR_2]^{\bullet+}$, comprising two-center three-electron (2c3e) bonds, which have been studied by quantum chemical calculations.[8–12] Besides fundamental interest, these species are small molecule models relevant for the pathogenesis of Alzheimer's disease, which involves methionine radical cation moieties interacting with the protein environment.[13–15] The life span of these dinuclear radical cations, $[R_2SSR_2]^{\bullet+}$, rarely exceeds milliseconds. The first notable exception involves the 1,5-dithiooctane radical cation **I**, which persists for several days due to the transannular S–S-bond (Figure 1).[16] More recently, the 1,8-bis(phenylsulfanyl)naphthalene radical cation **II** and its selenium analog were isolated and fully characterized by X-ray crystallography and EPR spectroscopy (Figure 1).[17,18] Besides the two-center three-electron (2c3e) bond stabilization, evidence was found that radical cations, $[R_2S]^{\bullet+}$, may also favorably interact with adjacent aromatic rings.[19,20] A series of *m*-terphenyl thio, seleno- and telluroethers, showed systematically lowered oxidation potentials, which were attributed to through-space chalcogen···π interactions in the related short-lived radical cations. For a related series of bis(*m*-terphenyl)dichalcogenide

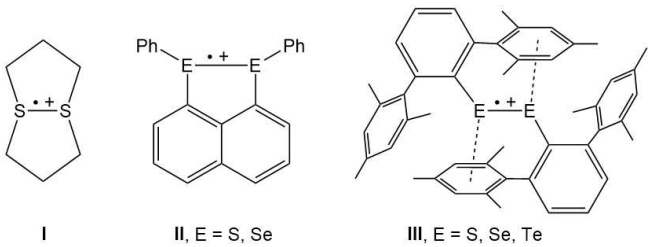

I **II**, E = S, Se **III**, E = S, Se, Te

Figure 1. Examples of dinuclear chalcogen radical cations.

[a] D. Duvinage, Dr. F. Mostaghimi, M. Damrath, J. Spils, P. Komorr, Prof. Dr. J. Beckmann
Institut für Anorganische Chemie und Kristallographie
Universität Bremen
Leobener Strasse 7, 28359 Bremen (Germany)
E-mail: j.beckmann@uni-bremen.de

[b] Dr. D. S. Odintsov, Prof. Dr. L. A. Shundrin
N. N. Vorozhtsov Institute of Organic Chemistry
Siberian Branch of Russian Academy of Sciences
Acad. Lavrentiev Avenue 9, 630090 Novosibirsk (Russia)
E-mail: shundrin@nioch.nsc.ru

[c] Prof. Dr. M. Fedin
Laboratory of Magnetic Resonance
International Tomography Center Siberian Branch of Russian Academy of Sciences
Institutskaya 3a, 630090 Novosibirsk (Russia)

[d] Dr. S. Mebs
Institut für Experimentalphysik
Freie Universität Berlin
Arnimallee 14, 14195 Berlin (Germany)
E-mail: stefan.mebs@fu-berlin.de

Supporting information for this article is available on the WWW under https://doi.org/10.1002/chem.202203498

radical cations **III** such chalcogen···π interactions were indeed structurally confirmed.[21] This observation raises the question whether the oxidation of extremely bulky bis(*m*-terphenyl)chalcogenides may similarly provide a route for the preparation for stable diorgano chalcogenide radical cations that resist electron stabilization via two-center three-electron (2c3e) bonds and formally contain 7 valence electrons.

Results and Discussion

The synthesis of the bis(*m*-terphenyl) chalcogenides, (2,6-$Mes_2C_6H_3)_2E$ (**1a**, E = S; **1b**, E = Se; **1c**, E = Te) turned out to be surprisingly difficult. After numerous failed attempts trying to adopt established routes for sterically less encumbered diaryl chalcogenides,[22] the preparation was eventually achieved by the reaction of the chalcogen tetrafluorides EF_4 (E = S, Se, Te) with three equivalents of the *m*-terphenyl lithium reagent, 2,6-

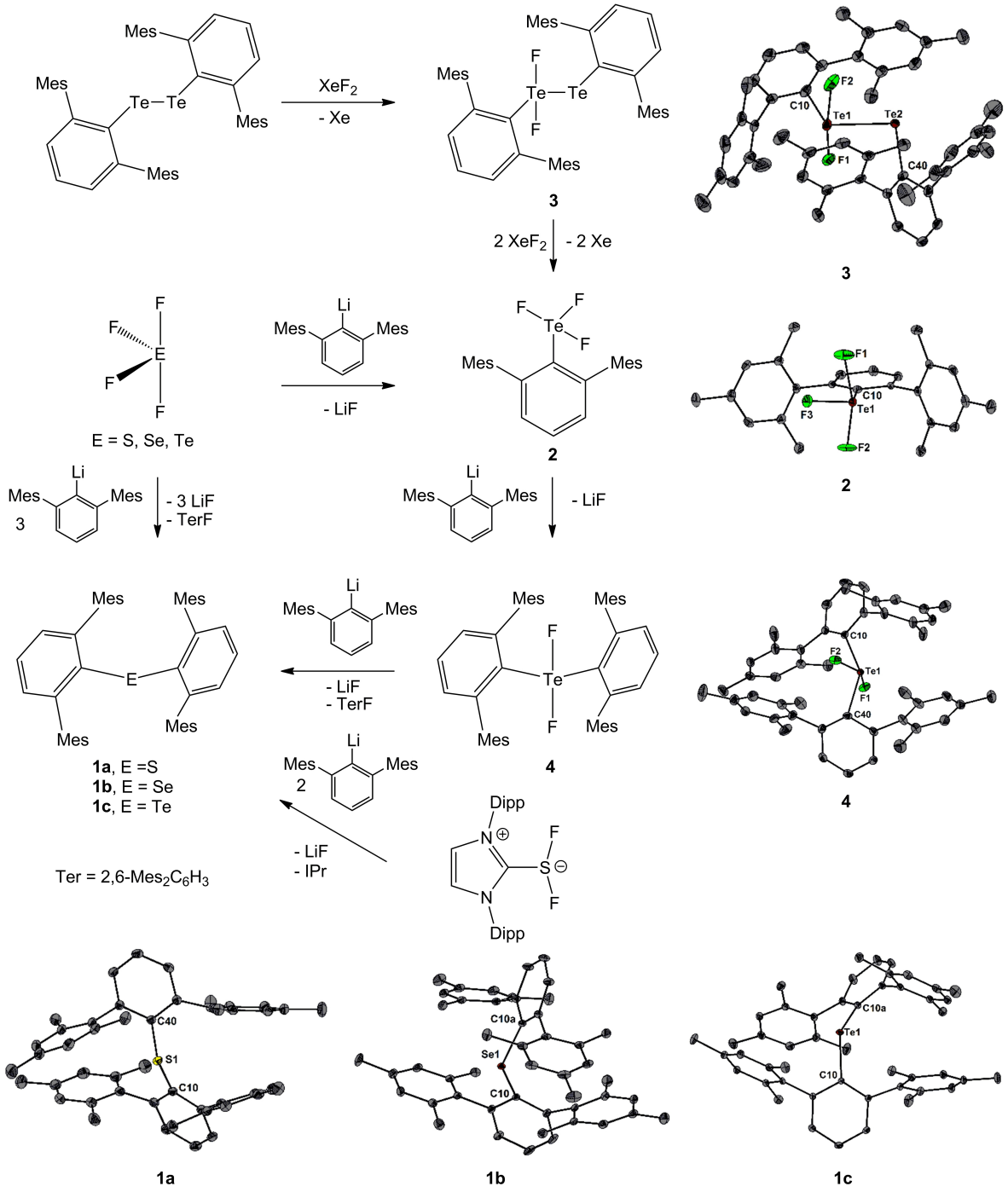

Figure 2. Synthesis of **1a–c** and **2–4**. Molecular structures of **1a–c** and **2–4**. Thermal ellipsoids set at 50% probability. Hydrogen atoms were omitted for clarity.

$Mes_2C_6H_3Li$, which fulfils two functions. The first two equivalents substitute two fluorine atoms by *m*-terphenyl groups at the chalcogen atom in the oxidation state IV. The last equivalent reduces the chalcogen to the oxidation state II. In this way, **1 a**, **1 b** were obtained as colorless and **1 c** as yellow crystals in 42, 64 and 52 % yield (Figure 2). Compounds **1 a** and **1 c** are indefinitely stable even when exposed to the air, whereas **1 b** slowly decomposes in the presence of moisture.[23] The two heavier bis-(*m*-terphenyl) chalcogenides were characterized by heteronuclear NMR spectroscopy. The ^{77}Se NMR spectrum of **1 b** shows a signal at $\delta = 981.0$ that is less shielded than those of Ph_2Se ($\delta = 422$)[24] and Mes_2Se ($\delta = 225$).[25] The ^{125}Te NMR spectrum of **1 c** exhibits a signal at $\delta = 572.0$ that lies midway between those of Ph_2Te ($\delta = 707$) and Mes_2Te ($\delta = 275$).[26]

The molecular structures of **1 a**, **1 b** and **1 c** show the large steric encumbrance of the bulky *m*-terphenyl substituents,[27] which, however, has only a small effect on the average E–C bond lengths (E = S, Se, Te) that are only slightly elongated compared to Mes_2S (1.787(1) vs. 1.785(1) Å),[28] Mes_2Se (1.944(4) vs. 1.931(1) Å)[29] and Mes_2Te (2.150(1) vs. 2.140(3) Å).[30] The effect is more pronounced for the C–E–C angles of **1 a**–**c**, which are considerably larger than those of Mes_2S (114.5(1) vs. 106.4(1)°),[28] Mes_2Se (116.1(2) vs. 102.0(1)°)[29] and Mes_2Te (116.2(2) vs. 101.0(1)°).[30]

We also studied the stepwise reaction of TeF_4 with 2,6-$Mes_2C_6H_3Li$ to shed light on the intermediates leading to the formation of **1 c**. At an equimolar ratio this reaction afforded the mono-substituted *m*-terphenyl tellurium trifluoride 2,6-$Mes_2C_6H_3TeF_3$ (**3**) in 61 % yield. In an effort to avoid TeF_4, the same product may also be obtained by fluorination of (2,6-$Mes_2C_6H_3$)TeTe(2,6-$Mes_2C_6H_3$) with XeF_2, which proceeds via the initial formation of mixed valent *m*-terphenyl tellurenyl fluoride (2,6-$Mes_2C_6H_3$)F_2TeTe(2,6-$Mes_2C_6H_3$) (**2**)[31,32] and eventually gives **3** in 42 % yield.[33] The reaction of 2,6-$Mes_2C_6H_3TeF_3$ (**3**) with 2,6-$Mes_2C_6H_3Li$ allows the introduction of a second *m*-terphenyl substituent at tellurium, following the formation of the bis-(*m*-terphenyl) tellurium difluoride (2,6-$Mes_2C_6H_3)_2TeF_2$ (**4**) in 53 % yield.[34] Interestingly, the C–Te–C bond angle of **4** (140.7(1)°)[27] is dramatically larger than those of **1 c** (116.2(2)°) and Mes_2TeF_2 (110.1(1)°),[35] which supposedly gives rise to a weaker repulsion between the two *m*-terphenyl substituents. The reaction of **4** with one equivalent of 2,6-$Mes_2C_6H_3Li$ indeed proceeded with reduction[36] of the tellurium giving rise to the telluride **1 c**, which confirms the mechanism proposed for the reaction of TeF_4 with three equivalents of 2,6-$Mes_2C_6H_3Li$ (see above). The major drawback of this method of preparation is the handling of highly corrosive and gaseous SF_4, which is not only needed as starting material for **1 a**, but also for the preparation of liquid SeF_4[37] and solid TeF_4[38] (from SeO_2 and TeO_2), the starting materials of **1 b** and **1 c**. Sulfur tetrafluoride, SF_4, often contains thionyl fluoride, $S(O)F_2$, as an impurity, which forms as a side product during the synthesis of SF_4, or by hydrolysis caused by traces of water. Due to their similar boiling points, SF_4 and $S(O)F_2$, cannot be separated by distillation. The reaction of three equivalents of 2,6-$Mes_2C_6H_3Li$ with mixtures of SF_4 and $S(O)F_2$ gave rise to inseparable mixtures of **1 a** and the sulfoxide, (2,6-$Mes_2C_6H_3)_2SO$.[39,40] Consequently, high purity of SF_4 was instrumental for the synthesis of **1 a** via this route. Therefore, we turned our attention to the reaction of the donor acceptor complex $IPrSF_2$ (IPr = 1,3-bis(2,6-diisopropylphenyl)imidazol-2-ylidene)[41] with two equivalents of the *m*-terphenyl lithium reagent, 2,6-$Mes_2C_6H_3Li$. Indeed, this reaction provides an alternative method for the preparation of **1 a**, which was isolated after column chromatography in 23 % yield.[22,42]

The electrochemical oxidation (ECO) of the bis(*m*-terphenyl) chalcogenides, studied by cyclic voltammetry in CH_2Cl_2, was irreversible for **1 a** and **1 b** at their half-wave potentials of $E_{1/2} =$ 1.59 and 1.22 V, respectively (Figure 3).[43] In contrast, the first ECO step of telluride **1 c** is a reversible one-electron and diffusion-controlled process ($E_{1/2} = 1.08$ V) associated with the formation of the corresponding long-lived radical cation $[\mathbf{1c}]^{\bullet+}$. The transition of the electron transfer kinetics to an irreversible process was observed for this ECO stage at increased potential sweep rates, starting from 400 mV s^{-1} (see the Supporting Information). The second ECO step of **1 c** is irreversible ($E_{peak} =$ 1.65 V) and is at least a two-electron process.[43] The ECO revealed a two-electron ECO process for **1 a** and a one-electron process for **1 b**, both in correlation with irreversible electron transfer kinetics (see the Supporting Information). The oxidation potentials suggest that the ionization potentials decrease in the order **1 a** > **1 b** > **1 c** (see DFT calculations below).

After examination of the redox properties, we studied the (single-electron) oxidation of the bis-(*m*-terphenyl) chalcogenides **1 a**–**1 c** using XeF_2 in the presence of $K[B(C_6F_5)_4]$.[44] While the reaction with **1 a** and 1**b** gave ill-defined dark mixtures even at low temperatures, the reaction of **1 c** provided a persistently blue solution, from which the radical cation salt [(2,6-$Mes_2C_6H_3)_2Te]^{\bullet+}[B(C_6F_5)_4]^-$, $[\mathbf{1c}]^{\bullet+}[B(C_6F_5)_4]^-$, was isolated as blue crystals in 96 % yield (Figure 4). In the solid-state, it is indefinitely stable under inert conditions. When exposed to the air, it is even stable for up to a week without signs of degradation. In solutions of chlorinated solvents such as CH_2Cl_2, it is stable for up to 3 months if the solvent is properly dried and degassed. In wet solvents a degradation is visible by loss of color over the course of an hour. The molecular structure of

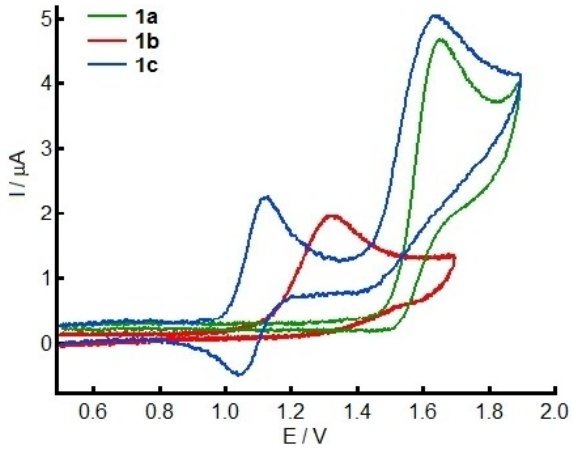

Figure 3. Normalized cyclic voltammograms of **1 a**–**1 c** in CH_2Cl_2. (Normalization to equal concentration of 1 mM, potential sweep rate was 0.1 V s^{-1}).

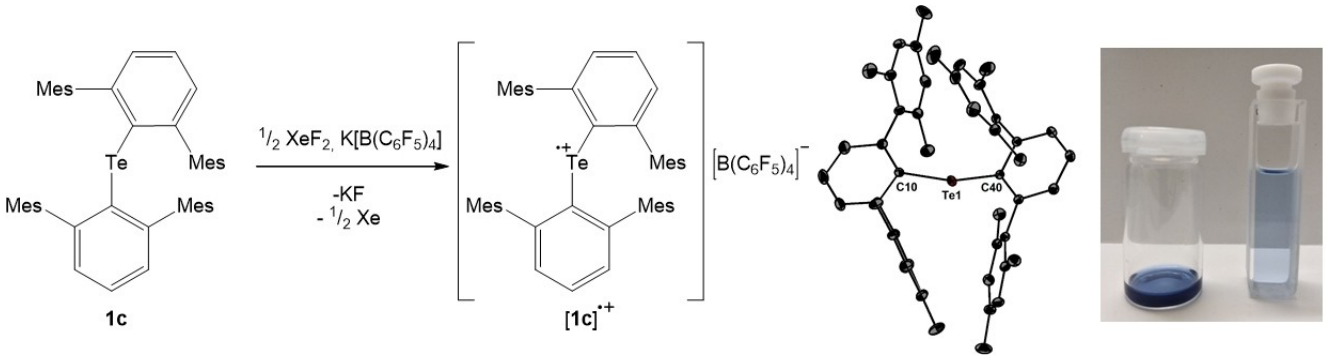

Figure 4. From left to right: Synthesis of the radical cation [**1 c**]$^{\bullet+}$ by oxidation of **1 c** with XeF_2 and $K[B(C_6F_5)_4]$. Molecular structure of [**1 c**]$^{\bullet+}$. Thermal ellipsoids set at 50% probability. Hydrogen atoms and the $[B(C_6F_5)_4]^-$ anion are omitted for clarity. Selected bond lengths and angles of [**1 c**]$^{\bullet+}$: Te1-C10 2.165(1) Å, Te1-C40 2.179(1) Å, C10-Te1-C40 114.9(1)°. A solution of [**1 c**]$^{\bullet+}$ (CH_2Cl_2 (50 μM) (left), CH_2Cl_2 (10 μM) (right)).

[**1 c**]$^{\bullet+}[B(C_6F_5)_4]^-$ shows clear ion separation.[27] This is in marked contrast to Roesky's bis(trimethylsilyl)amide tellurium radical cation $[\{(Me_3Si)_2N\}_2Te]^{\bullet+}[AsF_6]^-$, which is not only electronically stabilized by conjugation with the lone pairs at the N atoms, but is also affected by ion pairing.[45] In [**1 c**]$^{\bullet+}[B(C_6F_5)_4]^-$, the individual Te–C bond lengths (2.166(1) and 2.179(1) Å) are significantly different and surprisingly, the average value (2.173(1) Å) is somewhat larger than in the neutral parent **1 c** (2.150(1) Å). Even more surprising, the C–Te–C (114.9(1)°) slightly decreases compared to the neutral parent **1 c** (116.2(2)°), which is counterintuitive with respect to the loss of one electron. We note that the Te–N bond lengths of $[\{(Me_3Si)_2N\}_2Te]^{\bullet+}[AsF_6]^-$ are slightly shorter than in the neutral telluride $\{(Me_3Si)_2N\}_2Te$, which was attributed to the conjugation with the lone pairs at the N atoms.[45]

The radical cation [**1 c**]$^{\bullet+}$ was characterized by electron paramagnetic resonance (EPR) spectroscopy. Due to the extremely fast relaxation time, the EPR spectrum of [**1 c**]$^{\bullet+}$ was not observed in a liquid CH_2Cl_2 solution at room temperature and was measured in frozen glassy CH_2Cl_2 at 40 K using CW and spin echo detection modes (see the Supporting Information for details). The EPR spectrum at the X-band is characterized by a *g*-tensor with principal components of 1.9593, 2.0455, 2.2125 (Figure 5).

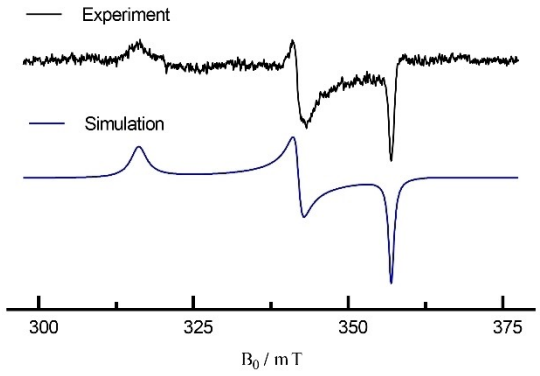

Figure 5. CW EPR spectrum of radical cation [1c]$^{\bullet+}$ in glassy CH_2Cl_2 at 40 K (upper spectrum) and its simulation (lower spectrum).

Compared to related bis(*m*-terphenyl)ditelluride radical cation $[(2,6\text{-}Mes_2C_6H_3Te)_2]^{\bullet+}$,[21] the *g*-tensor of [**1 c**]$^{\bullet+}$ has a smaller g_z component, while the values of g_x, g_y are comparable in magnitude. Unlike $[(2,6\text{-}Mes_2C_6H_3Te)_2]^{\bullet+}$, no hyperfine structure was observed for [**1 c**]$^{\bullet+}$ under the experimental conditions used (see the Supporting Information).

The radical cation [**1 c**]$^{\bullet+}$ was also characterized by NMR spectroscopy (see the Supporting Information for details). In the ^{1}H NMR spectrum, an increase of sterical restraint of the flanking mesityl substituents is observed, as the *meta* hydrogen atoms and *ortho* methyl groups of the mesityl substituents become magnetically inequivalent. This is caused by a steric restriction in rotation and leads to three signals with equal integral in the aliphatic region, as well as two signals with equal integral in the aromatic region for the *meta* hydrogen atoms of the mesityl ring. In the ^{13}C NMR spectrum the steric restraint is also visible in six mesityl assigned aromatic signals and three aliphatic signals, which were assigned to the methyl groups, even though the *ortho* methyl groups only differ slightly by their chemical shifts ($\Delta\delta = 0.04$ ppm). The signal of the *ipso* carbon is not visible in the ^{13}C NMR spectrum which might be attributed to spin density situated at the tellurium. This is consistent with the disappearance of the ^{125}Te NMR shift in an area of (−4000)–(+16000) ppm and the fact that the remaining signals in ^{1}H and ^{13}C NMR spectra are displayed as narrow, sharp signals without any broadening effects.

The radical cation [**1 c**]$^{\bullet+}$ was also characterized by UV-VIS-NIR spectroscopy using a 3D spectroelectrochemical technique (the Supporting Information). The differential spectroelectrochemical surface of the ECO of **1 c** obtained in CH_2Cl_2 with a triangular potential sweep in the range $0 < E < 1.5$ V ($0 < t <$ 700 s), showed a high reversibility of optical absorption consistent with the formation of radical cation [**1 c**]$^{\bullet+}$ (Figure 6a).

The optical absorption spectrum (Figure 6b) of [**1 c**]$^{\bullet+}$ is characterized by intense absorption bands in the near IR ($\lambda_1 =$ 951 nm), visible ($\lambda_2 = 693$ nm, $\lambda_3 = 613$ nm) and near UV area ($\lambda_4 = 339$ nm, $\lambda_5 = 284$ nm), resulting in an intense blue color of the corresponding solution (Figure 4).

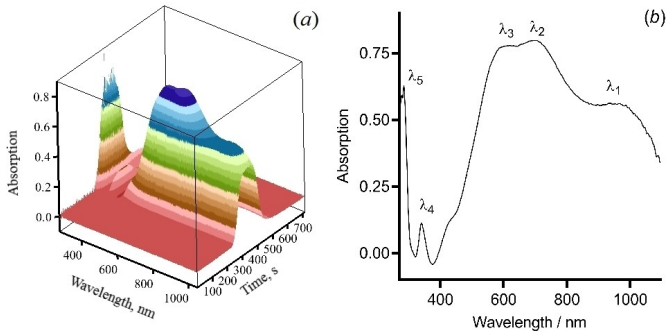

Figure 6. (a) 3D UV-VIS-NIR spectroelectrochemical surface of **1 c** oxidation in CH_2Cl_2, (b) maximum intensity optical absorption spectrum obtained at E = 1.4 V, t = 360 s.

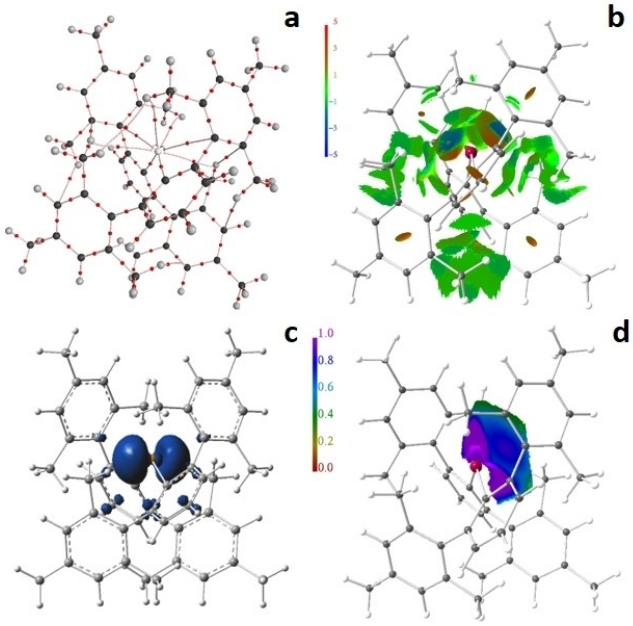

Figure 7. RSBI analysis of $[\mathbf{1c}]^{\bullet+}$. (a) AIM bond paths motif, (b) NCI *iso*-surface at s(**r**) = 0.5, (c) spin-density (SD) distribution at ϕ = 0.005 a.u., (d) ELI-D distribution mapped on the lone-pair basin of the Te atom.

The electronic structures of the neutral parents **1 a–c**, the radical cations $[\mathbf{1a–c}]^{\bullet+}$ as well as the dications $[\mathbf{1a–c}]^{2+}$ were determined by means of density functional theory (DFT) calculations and subsequent real-space bonding indicator (RSBI) analysis. RSBI included the Atoms-In-Molecules (AIM)[46] theory, the electron localizability indicator (ELI-D)[47] toolkit, as well as the noncovalent interactions (NCI)[48] index, providing topological, surface, and integrated bonding descriptors in real space. For the radical cations, the picture is complemented by inspection of the frontier orbitals and UV-VIS calculations employing time-dependent DFT (TD-DFT). All structures were fully optimized in the gas-phase. First and second vertical and adiabatic ionization energies (IE_v, IE_a) have been extracted, which follow the expected decrease along the series, for example IE_a = 649.6 kJ mol^{-1} (**1 a**), IE_a = 631.3 kJ mol^{-1} (**1 b**), IE_a = 592.2 kJ mol^{-1} (**1 c**) (Table S8). Notably, the geometric parameters of neutral parents **1 a–c**, the radical cations $[\mathbf{1a–c}]^{\bullet+}$ as well as the dications $[\mathbf{1a–c}]^{2+}$ do not follow clear trends in DFT, as they apparently are affected by weak intramolecular secondary interactions (Table S10). The primary E–C contact distance decreases with increased charge for Se (1.922→1.912→1.909 Å) and Te (2.125→2.121→2.115 Å), but is larger for $[\mathbf{1a}]^{2+}$ than for $[\mathbf{1a}]^{\bullet+}$ (1.768→1.755→1.761 Å). Similarly, the largest C–E–C angle is found for the radical cations $[\mathbf{1b}]^{\bullet+}$ and $[\mathbf{1c}]^{\bullet+}$, but for the neutral [**1 a**]. It is not surprising that the experimental structural findings for $[\mathbf{1c}]^{\bullet+}$ are not well reflected in DFT, as the geometric parameters are likely also sensitive against the effect on weak inter-molecular secondary interactions. In contrast to the X-ray structure, $[\mathbf{1c}]^{\bullet+}$ almost obeys C_2-symmetry (unrestrained optimization) in DFT, the Te–C bond distance has decreased compared to **1 c**, and the C–Te–C angle was widened from 101.5 to 119.2°. The AIM bond topology, NCI contact patches, spin-density (SD) distribution, and electron localizability distribution mapped on the ELI-D lone-pair (LP) basin of the Te atom in $[\mathbf{1c}]^{\bullet+}$ are displayed in Figure 7.[49]

The AIM topology discloses four secondary Te···H as well as two Te···C_π contacts (Figure 7a), characterized by bond critical points (bcps, red dots) in the electron density (ED, ρ(**r**)). The spatial extension of these contacts is visible in the NCI, largely covering the coordination space around the central atom (Figure 7b), highlighting their role for kinetic stabilization of the radical. The rather localized blueish areas in the NCI and the disc-shaped area of increased localizability in the ELI-D (Figure 7d) reflect the attractive interaction between the chalcogen atom and the π-electron density of the mesityl side groups. Similar results were obtained for the bis-(*m*-terphenyl) element cations $[(2,6\text{-}Mes_2C_6H_3)_2E]^+$ of group 13[50] and 15[51] formally possessing 4 and 6 valence electrons.

The quantitative AIM bond parameters (Tables S11 and S12) characterize the primary E–C (E = S, Se, Te) bonds to be of polarized-covalent nature with medium charge accumulations at the E–C bpcs (ρ(r) = 0.8–1.4 eÅ^{-3}) and a (slightly) negative Laplacian of the ED ($\nabla^2\rho(\mathbf{r}) = -8$ to about 0 eÅ^{-5}). The total energy density over ED ratio (H/ρ(**r**)) is considerably negative, reflecting covalency, and moreover being larger in absolute numbers than the kinetic energy density over ED ratio (G/ρ(**r**)), suggesting (slight) dominance of covalent over ionic bonding aspects (Table S11). Bond ellipticities (ε) of about 0.1 indicate minor distortions from cylindrical ED accumulation at the bcp, thus bending or 'smearing'. To the contrast, all secondary intramolecular interactions are of the Van-der-Waals type, with low ED values at the bcps of 0.06–0.21 eÅ^{-3}, (slightly) positive Laplacians, and clearly dominating G/ρ(**r**) ratios. H/ρ(**r**) in most cases is even slightly positive, indicating the total absence of covalent bond contributions. Ellipticities of up to 2.8 are caused by electron smearing along the considerably bent Te···H and Te···C_π bond paths. Whereas oxidation goes along with increased AIM charges for one-electron oxidation, it rather goes to the expense of substituent charge in the second oxidation (Table S10). In the ELI-D picture, one electron oxidation causes the transfer of electron population ($N_{(ELI)}$) from the LP(E) basins

towards the E–C bonding basins, resulting in almost inverted $N_{(ELI)}$ values between neutral and cationic counterparts. Electron loss is accompanied by decrease of ELI-D basin volume and decreased localizability (γ) and *vice versa* (Table S10). As an exception, the Te–C basins also show reduced localizability after oxidation. In accordance with the AIM charges of the chalcogen atoms, little changes are observed for the chalcogen-related ELI-D basins after the second oxidation.

The p_z-shaped SD around the Te atom shows a very low level of delocalization and polarization, suggesting that the terphenyl substituents are electronically innocent (Figure 7c and Figure S53c). A slightly larger level of delocalization of spin density into the ligand system is obtained for the $[\{(Me_3Si)_2N\}_2Te]^{\bullet+}$ radical cation in an otherwise similar overall SD distribution (Figure S53d). The ELI-D localization domain representation of $[\{(Me_3Si)_2N\}_2Te]^{\bullet+}$ unravels two LP-basins, which are still fused at an *iso*-value of 1.4, mirroring the p_z(Te)-shaped SD, thereby not supporting the proposed 'rehybridization'[45] of the non-bonding electrons. Similar ELI-D figures are obtained for the three radical cations [(2,6-$Mes_2C_6H_3)_2E]^+$ [**1 a–c**]$^{\bullet+}$. In case of E = S the two LP(E)-basins are topologically fused for all three oxidation states (Figure S54g-i). In contrast, they are separated for the neutral **1 b** and **1 c**, but fuse after extraction of one electron (Figures S55g–h and S56 g–h). In case of E = Te, this goes to the extreme for the dication [**1 c**]$^{2+}$ as the formerly two LP(Te) basins fully fuse to form a single ELI-D basin (Figure S56i). This suggests that the local electronic environment around the Te atom shows stronger effects against one or two electron oxidation than the lighter analogues.

Inspection of the frontier orbital energies uncovers comparable HOMO-LUMO gaps of 0.17–0.18 a.u. for the neutral compounds **1 a–c** (Table S9). One electron oxidation drops the energies of the α-HOMOs, α-LUMOs, and β-HOMOs by about 0.11–0.15 a.u. (ΔE), but the energies of the β-LUMOs by about 0.25 a.u., decreasing the gap between β-HOMO and β-LUMO to about 0.04 a.u. for [**1 a**]$^{\bullet+}$, 0.05 a.u. for [**1 b**]$^{\bullet+}$, 0.06 a.u. for [**1 c**]$^{\bullet+}$, shifting the transitions into the UV/vis area. In the radical cations, the β-HOMOs are dominated by contributions from the *m*-terphenyl π-electron densities, whereas the β-LUMOs are dominated by p_z(E) contributions. Notably, the α-HOMOs are dominated by contributions of the substituents in [**1 a**]$^{\bullet+}$ and [**1 b**]$^{\bullet+}$, and only [**1 c**]$^{\bullet+}$ shows p_z(Te)-like contributions, which is in contrast to the picture obtained for the $[\{(Me_3Si)_2N\}_2Te]^{\bullet+}$ radical cation in which both α-HOMO and β-LUMO are dominated by p_z(Te)-like contributions (Figure S9). For [**1 a**]$^{\bullet+}$ and [**1 b**]$^{\bullet+}$, p_z(Te) character is contributing to the HOMO-1 orbitals. UV/vis transitions were computed for [**1 a–c**]$^{\bullet+}$ employing TD-DFT, (Figure S57 and Tables S13-S15). Considerable oscillator strengths are obtained for [**1 c**]$^{\bullet+}$ at 620 and 770 nm, matching very well with the experimental data (Figure 6). All donor orbitals are associated with the substituents and of π-character, whereas the acceptor orbital is p_z(Te)-like in [**1 c**]$^{\bullet+}$, pointing to a substituent-to-chalcogen transition. Comparable transitions are obtained for [**1 a**]$^{\bullet+}$ and [**1 b**]$^{\bullet+}$, but significantly red-shifted as the first relevant transitions occur at close to 1000 nm. Single-reference techniques are known to be problematic for open-shell systems,[52] so the UV-VIS calculations are at best semi-quantitative.

Conclusion

The one-electron oxidation of the extremely bulky bis(*m*-terphenyl) telluride, $(2,6\text{-}Mes_2C_6H_3)_2Te$ (**1 c**) was the key to the preparation of the first kinetically stabilized radical cation $(2,6\text{-}Mes_2C_6H_3)_2Te][B(C_6F_5)_4]$ ([**1 c**][$B(C_6F_5)_4$]). A related species was recently postulated as intermediate in a catalytic Te(II)/Te(III) cycle.[53] The spin density of [**1 c**]$^{\bullet+}$ is almost exclusively situated at the Te atom, unlike in Roesky's $[\{(Me_3Si)_2N\}_2Te]^{\bullet+}$ radical cation, which is electronically stabilized and comprises spin density also at the N atoms.[45] The oxidation of the lighter analogues $(2,6\text{-}Mes_2C_6H_3)_2E$ (**1 a**, E = S; **1 b**, E = Se) provided only ill-defined decomposition products.

Experimental Section

Synthesis and characterization of $(2,6\text{-}Mes_2C_6H_3)_2S$ (1 a)

Method A: $2,6\text{-}Mes_2C_6H_3Li$ (1.60 g, 5.00 mmol, 1.00 equiv) was placed in a Schlenk tube, to this Et_2O (60 mL) was added and the solution was cooled to −78 °C. To this sulfur tetrafluoride (8.00 g, 7.36 mmol, 14.8 equiv) was condensed and the reaction was slowly warmed to room temperature. After 18 h, the solvent was removed under reduced pressure. To the remaining residue $2,6\text{-}Mes_2C_6H_3Li$ (1.60 g, 5.00 mmol, 1.00 equiv) was added and the solids were cooled to −78 °C. Et_2O (50 mL) was added and the reaction mixture was again slowly warmed up to room temperature over the course of 18 h. The solvent was removed under reduced pressure and the remaining solid was dissolved in CH_2Cl_2 (50 mL) and worked up aqueous (3 × 50 mL). After removal of CH_2Cl_2 the crude product was separated by column chromatography (cyclohexane: toluene 4 : 1, $R_f = 0.6$). After removal of the solvent under reduced pressure **1 a** was obtained as a colorless solid (1.38 g, 42 %).

Method B: $2,6\text{-}Mes_2C_6H_3Li$ (256 mg, 0.76 mmol, 1.00 equiv) and $IPrSF_2$ (183 mg, 0.359 mmol, 0.50 equiv) were placed in a Schlenk tube and cooled to −78 °C. To this toluene (8 mL) was slowly added and the reaction was stirred for 30 minutes at −78 °C. The cooling bath was removed and the reaction mixture was stirred for additional 20 h. The solvent was removed under reduced pressure. The residue was washed with ethanol (3 × 10 mL) and *n*-hexane (3 × 10 mL). The residual off white solid was separated by column chromatography (cyclohexane: toluene 4 : 1, $R_f = 0.6$). After removal of the solvent under reduced pressure **1 a** was obtained as a colorless solid (54.4 mg, 23 %).

Crystals suitable for X-Ray diffraction measurements were grown by cooling down a hot solution of **1 a** a minimum amount of heptane.

^{1}H NMR (600 MHz, $CDCl_3$): $\delta = 7.02$ (t, $^3J(^1H\text{-}^1H) = 7.6$ Hz, 2H, H4), 6.74 (d, $^3J(^1H\text{-}^1H) = 7.6$ Hz, 4H, H3 and H5), 6.73 (s, 8H, H9 and H11), 2.36 (s, 12H, H14), 1.64 (s, 24H, H13 and H15) ppm. **$^{13}C\{^1H\}$ NMR (151 MHz, $CDCl_3$)**: $\delta = 145.4$ (s, C2 and C6), 138.8 (s, C7), 136.8 (s, C8 and C12), 136.2 (s, C10), 134.9 (s, C1), 131.6 (s, C3 and C5), 128.3 (s, C9 and C11), 126.5 (s, C4), 21.4 (s, C13 and C15), 21.3 (s, C14) ppm. **HRMS ESI (m/z)**: $[M+H]^+$ calculated. for $C_{48}H_{51}S$, 659.37060; found, 659.36925; $[M+Na]^+$ calculated for $C_{48}H_{50}SNa$, 681.35254; found, 681.35110; $[M+K]^+$ calculated for $C_{48}H_{50}SK$ 697.32648; found

697.32489. $[M\text{-}C_{24}H_{25}]^+$ calculated for $C_{24}H_{25}S$, 345.16175; found 345.16676.

Synthesis and characterization of (2,6-$Mes_2C_6H_3$)$_2$Se (1 b): 2,6-$Mes_2C_6H_3Li$ (572 mg, 1.79 mmol, 1.00 equiv) was charged in a Schlenk tube and dissolved in Et_2O (20 mL) and cooled to −78 °C. To this SeF_4 (0.10 mL, 1.79 mmol, 1.00 equiv) was added dropwise. The solution was slowly warmed to room temperature and the solvent was removed under reduced pressure. To the residue 2,6-$Mes_2C_6H_3Li$ (1.14 g, 3.58 mmol, 2.00 equiv) was added and the Schlenk tube was cooled to −78 °C. To this Et_2O (40 mL) was added and the suspension was stirred for one hour at −78 °C and then slowly warmed up to room temperature. The solvent was removed under reduced pressure and the residue dissolved in CH_2Cl_2 (50 mL) and worked up aqueous (3×50 mL). The organic phase was separated and dried over sodium sulphate. After removal of the solvent the crude product was separated by column chromatography (cyclohexane: ethyl acetate 9:1, R_f = 0.2). After removal of the solvent the residual yellow oil was triturated with *n*-pentane until the product crystallized. After decantation and drying under reduced pressure **1 b** was obtained as a colorless solid (241 mg, 64 %).

Crystals suitable for X-Ray diffraction measurements were grown by diffusion of *n*-hexane into a CH_2Cl_2 solution of **1 b**.

^{1}H NMR (600 MHz, $CDCl_3$): δ = 7.30 (t, $^3J(^1H\text{-}^1H)$ = 7.5 Hz, 1H, H4), 6.82 ((d, $^3J(^1H\text{-}^1H)$ = 7.5 Hz, 2H, H3 and H5), 6.76 (s, 4H,H9 and H11), 2.34 (s, 6H, H14), 1.75 (s, 6H, H13), 1.72 (s, 6H, H15) ppm.**^{13}C{^{1}H} NMR (151 MHz, CD_2Cl_2)**: δ = 144.3 (s, C2 and C6), 143.6 (s, C1), 137.71 (s, C7), 137.3 (s, C12), 136.9 (s, C10), 136.5 (s, C8), 133.2 (s, C3 and C5), 129.9 (s, C4), 128.6 (s, C9), 128.5 (s, C11), 22.3 (s, C13), 22.1 (s, C15), 21.1 (s, C14) ppm. **^{77}Se NMR (CD_2Cl_2, 115 MHz)**: δ = 981.0 ppm. **HRMS ESI (m/z)**: $[M+OH]^+$ calculated. for $C_{48}H_{51}OSe$, 723.30996; found, 723.30921.

Synthesis and characterization of (2,6-$Mes_2C_6H_3$)$_2$Te (1c): TeF_4 (204 mg, 1.0 mmol, 1.00 equiv) was placed in a Schlenk tube, Et_2O (5 mL) was added and cooled to −78 °C. To this a solution of 2,6-$Mes_2C_6H_3Li$ (320 mg, 1.0 mmol, 1.00 equiv) in Et_2O (10 mL) was added dropwise and the suspension was stirred for one hour. After this, additional 2,6-$Mes_2C_6H_3Li$ (640 mg, 2.0 mmol, 2.00 equiv) was added and the reaction was slowly warmed up to room temperature and stirred for 18 h. The solvent was removed under reduced pressure and the residue was dissolved in CH_2Cl_2 (10 mL). The suspension was filtered through a PTFE syringe filter and the solvent of the filtrate was removed under reduced pressure. The remaining solid was washed with MeCN (3×5 mL) and dried under reduced pressure to obtain 1c as a yellow solid (367 mg, 52 %).

Crystals suitable for X-Ray diffraction measurements were grown by evaporation from a solution of **1 c** in CH_2Cl_2/hexane.

^{1}H NMR (600 MHz, $CDCl_3$): δ = 7.14 (t, $^3J(^1H\text{-}^1H)$ = 7.5 Hz, 1H, H4), 6.80 (s, 4H, H9 and H11), 6.76 (d, $^3J(^1H\text{-}^1H)$ = 7.5 Hz, 2H, H3 and H5), 2.36 (s, 6H, H14), 1.70 (s, 12H, H13 and H15) ppm.**^{13}C{^{1}H} NMR (151 MHz, $CDCl_3$)**: δ = 148.8 (s, C2 and C6), 142.1 (s, C7), 136.3 (s, C10), 136.1 (s, C8 and C12), 129.2 (s, C3 and C5), 128.1 (s, C9 and C11), 128.0 (s, C4), 119.9 (s, C1), 21.5 (s, C13 and C15), 21.4 (s, C14) ppm. **^{125}Te NMR ($CDCl_3$, 189 MHz)**: δ = 572.0 ppm. **HRMS ESI (m/z)**: $[M+Na]^+$ calculated. for $C_{48}H_{50}TeNa$, 779.28727; found, 779.28612.

Synthesis and characterization of 2,6-$Mes_2C_6H_3TeF_3$ (2)

Method A: (2,6-$Mes_2C_6H_3$)$_2$Te$_2$ (220 mg, 0.25 mmol, 1.00 equiv) was dissolved in CH_2Cl_2 (4 mL) and cooled to −78 °C. To this XeF_2 (127 mg, 0.75 mmol, 3.00 equiv) was added. The reaction mixture was slowly warmed to room temperature and stirred for 18 h. The solvent was removed under reduced pressure and the residue extracted with MeCN (3×5 mL). The solvent was removed under reduced pressure and the residue was dissolved in hot *n*-heptane (20 mL), upon cooling the title compound crystallized out. The supernatant was removed via syringe and the residual crystalline solid dried under reduced pressure to obtain **2** as a colorless crystalline solid (102 mg, 42 %).

Method B: 2,6-$Mes_2C_6H_3Li$ (360 mg, 1.00 mmol, 1.00 equiv) was placed in a Schlenk tube, dissolved in Et_2O (10 mL) and cooled to −78 °C. To this, TeF_4 (204 mg, 1.00 mmol, 1.00 equiv) was added and the suspension was slowly warmed up to room temperature and stirred for 18 h. After this, the solvent was removed under reduced pressure and the residual solid was dissolved in CH_2Cl_2 (5 mL) and the suspension was filtered through a PTFE syringe filter. The solvent of the filtrate was removed under reduced pressure and the remaining solid was dissolved in hot *n*-heptane (20 mL) and upon cooling the title compound crystallized out. The residual solvent was decanted off, and the residual solid was dried under reduced pressure to obtain **2** as a colorless crystalline solid (303 mg, 61 %).

Crystals suitable for X-Ray diffraction measurements were grown by slow cooling of a hot saturated *n*-heptane solution of **2**.

^{1}H NMR (600 MHz, CD_2Cl_2): δ = 7.71 (t, $^3J(^1H\text{-}^1H)$ = 7.6 Hz, 1H, H4), 7.33 (t, $^3J(^1H\text{-}^1H)$ = 8.2 Hz, 2H, H3 and H5), 7.07 (s, 2H, H9 and H11), 6.92 (s, 2H, H19 and H21), 2.37 (s, 3H, H15), 2.32 (s, 3H, H25), 2.12 (s, 6H, H13 and H15), 2.06 (s, 6H, H23 and H25) ppm. **^{13}C{^{1}H} NMR (151 MHz, CD_2Cl_2)**: δ = 150.5 (s, C1), 144.3 (s, C2), 142.9 (s, C6), 142.2 (s, C10), 140.1 (s, C8 and C12), 138.0 (s, C20), 137.4 (s, C18 and C22), 134.8 (s, C17), 133.6 (s, C7), 133.1 (s, C3), 133.1 (s, C4), 129.8 (s, C9 and C11), 129.7 (s, C5), 128.0 (s, C19 and C21), 21.6 (s, C14), 21.4 (s, C24), 21.0 (s, C13, C15, C23 and C25) ppm. **^{19}F NMR (565 MHz, CD_2Cl_2)**: δ = −59.2 (d ($^2J(^{19}F\text{-}^{19}F)$ = 31.1 Hz), −125.3 (t ($^2J(^{19}F\text{-}^{19}F)$ = 31.1 Hz) ppm. **^{125}Te NMR (189 MHz, CD_2Cl_2)**: δ = 1635.7 (dt, $^1J(^{125}Te\text{-}^{19}F)$ = 2285.97, 313.84 Hz) ppm. **HRMS ESI (m/z)**: $[M+Na]^+$ calculated. For $C_{24}H_{25}F_3NaTe$ 523.08683; found, 523.08594.

Synthesis and characterization of (2,6-$Mes_2C_6H_3$)$_2$Te$_2$F$_2$ (3): (2,6-$Mes_2C_6H_3$)$_2$Te$_2$ (212 mg, 0.5 mmol, 1.00 equiv) was placed in a Schlenk tube, to this CH_2Cl_2 (4 mL) was added and the solution was cooled to −78 °C. To this XeF_2 (320 mg, 1.0 mmol, 2.00 equiv) was added and the reaction was warmed to −40 °C and stirred for 2 h. The solvent was removed under reduced pressure to obtain a deep red solid. Monitoring by means of ^{19}F and ^{125}Te NMR spectroscopy showed 3 as a major species but also decomposition at room temperature in solution. Attempts to measure ^{1}H and ^{13}C spectra lead only to impure spectra due to decomposition in solution.

Crystals suitable for X-Ray diffraction measurements were grown by diffusion of hexane into a solution of **3** in CH_2Cl_2 at −30 °C.

^{19}F NMR (565 MHz, CD_2Cl_2): δ = −95.0 ppm. **^{125}Te NMR (189 MHz, CD_2Cl_2)**: δ = 1519.2 (td, $J(^{125}Te\text{-}^{19}F)$ = 1130.5 Hz), 1210.8 (t, $J(^{125}Te\text{-}^{19}F)$ = 72.5 Hz) ppm.

Synthesis and characterization of (2,6-$Mes_2C_6H_3$)$_2$TeF$_2$ (4)

Method A: TeF_4 (101 mg, 0.50 mmol, 1.00 equiv) and 2,6-$Mes_2C_6H_3Li$ (160 mg, 0.50 mmol, 1.00 equiv) were placed in a Schlenk tube and cooled to −78 °C. To this Et_2O (5 mL) was added and the reaction mixture was stirred for 1 h at −78 °C. After stirring for an hour 2,6-$Mes_2C_6H_3Li$ (160 mg, 0.50 mmol, 1.00 equiv) was added and the reaction mixture was slowly warmed to room temperature and stirred for 18 h. After this, the solvent was removed under reduced pressure and the residue was dissolved in CH_2Cl_2 (4 mL). The suspension was filtered via a PTFE syringe filter and the solvent of

the filtrate was removed under reduced pressure. The remaining solid was washed with MeCN (3×5 mL) and *n*-hexane (3×5 mL) and the solid was dried under reduced pressure to obtain **4** as a colorless solid (241 mg, 64%).

Method B: 2,6-$Mes_2C_6H_3TeF_3$ (249 mg, 0.50 mmol, 1.00 equiv) and 2,6-$Mes_2C_6H_3Li$ (160 mg, 0.50 mmol, 1.00 equiv) were placed in a Schlenk tube and cooled with an ice bath. To this, n-hexane (5 mL) is added and the reaction mixture is stirred for 72 h at room temperature. The solvent was removed under reduced pressure and the residue was dissolved in CH_2Cl_2 (4 mL). The reaction mixture was filtered via a PTFE syringe filter and the solvent was removed under reduced pressure. The residual solid was washed with MeCN (3×5 mL) and n-hexane (3×5 mL) and dried extensively to obtain **4** as a colorless solid (210 mg, 53%).

Crystals suitable for X-Ray diffraction measurements were grown from a hot solution of **4** in heptane.

^{1}H NMR (600 MHz, $CDCl_3$): $\delta = 7.30$ (t, $^3J(^1H\text{-}^1H) = 7.16$ Hz, 2H, H4), 6.83 (d, $^3J(^1H\text{-}^1H) = 7.0$ Hz, 4H, H3 and H5), 6.80 (s, 2H, H9 and H11), 2.42 (s, 6H, H14), 1.65 (s, 12H, H13 and H15) ppm. **$^{13}C\{^1H\}$ NMR (151 MHz, $CDCl_3$)**: $\delta = 151.9$ (s, C1), 144.6 (s, C2 and C6), 138.3 (s, C7), 137.8 (s, C8 and C12), 136.7 (s, C10), 131.1 (s, C3 and C5), 130.4 (s, C10), 128.1 (s, C9 and C11), 21.4 (s, C14), 20.7 (s, C13 and C15) ppm. **^{19}F NMR ($CDCl_3$, 565 MHz)**: $\delta = -103.1$ ppm. **^{125}Te NMR ($CDCl_3$, 189 MHz)**: $\delta = 1289.2$ (t, $^1J(^{125}Te\text{-}^{19}F) = 313.6$ Hz) ppm. **HRMS ESI (m/z)**: $[M-F]^+$ calculated. for $C_{48}H_{50}FTe$, 775.29533; found, 775.29481; $[M+Na]^+$ calculated. For $C_{48}H_{50}F_2NaTe$ 817.28350; found, 817.28274; $[M+K]^+$ calculated. For $C_{48}H_{50}F_2KTe$ 833.25744; found, 833.25652.

Synthesis and characterization of $[(2,6\text{-}Mes_2C_6H_3)_2Te][B(C_6F_5)_4]$ ($[1c]^{\bullet+}[B(C_6F_5)_4]^-$): 1c (49.0 mg, 65 μmol, 1.00 equiv) and $K[B(C_6F_5)_4]$ (45.5 mg, 65 μmol, 1.00 equiv) were placed in a Schlenk tube, to this CH_2Cl_2 (4.00 mL) was added and the suspension was cooled to −78 °C. To this XeF_2 (5.50 mg, 32.5 μmol, 0.50 equiv) was added. The solution was slowly warmed up to room temperature and stirred for additional 48 h. The deep blue solution was filtered and layered with *n*-hexane (20 mL). The crystallized compound was washed with *n*-hexane (2×5 mL) and dried under reduced pressure to obtain 1c as deep blue crystalline solid (89.2 mg, 96%).

Crystals suitable for X-Ray diffraction measurements were grown by diffusion from a solution of **1 c** in CH_2Cl_2 with *n*-hexane.

^{1}H NMR (600 MHz, CD_2Cl_2): $\delta = 7.73$ (t, $^3J(^1H\text{-}^1H) = 7.5$ Hz, 1H, H4), 7.2 (d, $2^3J(^1H\text{-}^1H) = 7.5$ Hz, 2H, H3 and H5), 6.97 (s, 2H, H9 or H11), 6.95 (s, 2H, H9 or H11), 4.70 (s, br, 7 H, CH_2Cl_2 coordinated), 2.37 (s, 6H, H14), 1.86 (s, 6H, H15), 1.65 (s, 6H, H13) ppm. **$^{13}C\{^1H\}$ NMR (151 MHz, CD_2Cl_2)**: $\delta = 148.7$ (d, $^1J(^{13}C\text{-}^{19}F) = 235.4$ Hz, br, C_6F_5), 147.6 (s, C2 and C6), 141.8 (s, C7), 138.8 (d, $^1J(^{13}C\text{-}^{19}F) = 245.2$ Hz, br, C_6F_5), 139.0 (s, C8), 137.9 (s, C12), 136.9 (d, $^1J(^{13}C\text{-}^{19}F) = 235.4$ Hz, br, C_6F_5), 136.1 (s, br, C4), 134.7 (s, C3 and C5), 134.1 (s, C10), 130.3 (s, C9), 129.8 (s, C11), 22.1 (s, C15), 22.0 (s, C13), 21.7 (s, C14) ppm. **$^{11}B\{^1H\}$ NMR (CD_2Cl_2, 193 MHz)**: $\delta = -16.5$ ($B(C_6F_5)_4$) ppm. **^{19}F NMR (CD_2Cl_2, 565 MHz)**: $\delta = -132.9$ (s, br, 2F, *o*-C_6F_5), −163.6 (t, $^3J(^{19}F\text{-}^{19}F) = 20.4$ Hz, 1F, *p*-C_6F_5), −167.4 (t, $^3J(^{19}F\text{-}^{19}F) = 17.8$ Hz, 2F, *m*-C_6F_5) ppm. **^{125}Te NMR (CD_2Cl_2, 189 MHz)**: δ = no visible signal from (−4000)–(+16000) ppm. **HRMS ESI (m/z)**: $[M+OH]^+$ calculated. for $C_{48}H_{51}OTe$, 773.29967; found, 773.29850. **UV-Vis (CH_2Cl_2, 10 μM)** λ(abs) = 350, 613, 707, 951 nm.

Acknowledgements

The Deutsche Forschungsgemeinschaft (Project BE 3716/6-2) and Russian Science Foundation (Project 22-13-00108) are gratefully acknowledged for financial support. Open Access funding enabled and organized by Projekt DEAL.

Conflict of Interest

The authors declare no conflict of interest.

Data Availability Statement

The data that support the findings of this study are available from the corresponding author upon reasonable request.

Keywords: chalcogenes · *m*-terphenyl · radical cations · tellurium

[1] P. P. Power, *Chem. Rev.* **2003**, *103*, 789–810.
[2] Z. Feng, S. Tang, Y. Su, X. Wang, *Chem. Soc. Rev.* **2022**, *51*, 5930–5973.
[3] R. S. Glass, Sulfur Radical Cations, *Top. Curr. Chem.* **1999**, *205*, 1–87.
[4] T. Nishinaga, K. Komatsu, *Org. Biomol. Chem.* **2005**, *3*, 551–569.
[5] L. V. Shuvaev, J. Passmore, *Coord. Chem. Rev.* **2013**, *237*, 1067–1091.
[6] R. S. Glass, Sulfur Radicals and Their Applications, *Top. Curr. Chem.* **2018**, *376*, 22.
[7] O. Lanzalunga, A. Lapi, *J. Sulfur Chem.* **2012**, *33*, 101–129.
[8] Y. Deng, A. J. Illies, M. A. James, M. L. McKee, P. Peschke, *J. Am. Chem. Soc.* **1995**, *117*, 420–428.
[9] F. M. Bickelhaupt, A. Diefenbach, S. P. de Visser, L. J. de Koning, N. M. M. Nibbering, *J. Phys. Chem. A* **1998**, *102*, 9549–9553.
[10] C. H. Hendon, D. R. Carbery, A. Walsh, *Chem. Sci.* **2014**, *5*, 1390–1395.
[11] D. Wang, A. Fuji, *Chem. Sci.* **2017**, *10*, 7260–7268.
[12] D. Wang, K. Hattori, A. Fujii, *Chem. Sci.* **2019**, *10*, 7260.
[13] C. Schönreich, D. Pogocki, G. L. Hug, K. Bobrowski, *J. Am. Chem. Soc.* **2003**, *125*, 13700–13713.
[14] D. A. Butterfield, D. Boyd-Kimball, *Biochim. Biophys. Acta* **2005**, 149–156.
[15] T. Quiñones-Ruiz, M. F. Rosario-Alomar, K. Ruiz-Esteves, M. Shanmugasundaram, V. Grigoryants, C. Scholes, J. López-Garriga, I. K. Lednev, *J. Am. Chem. Soc.* **2017**, *139*, 9755–9758.
[16] W. K. Musker, T. L. Wolford, *J. Am. Chem. Soc.* **1976**, *98*, 3055–3056.
[17] S. Zhang, X. Wang, Y. Sui, X. Wang, *J. Am. Chem. Soc.* **2014**, *136*, 14666–14669.
[18] S. Zhang, X. Wang, Y. Sui, Y. Qiu, Z. Zhang, X. Wing, *Nat. Commun.* **2014**, *5*, 4127.
[19] M. Ammam, U. I. Zakai, G. S. Wilson, R. S. Glass, *Pure Appl. Chem.* **2010**, *82*, 555–563.
[20] N. P.-A. Monney, T. Bally, T. Yamamoto, R. S. Glass, *J. Phys. Chem. A* **2015**, *119*, 12990–12998.
[21] O. Mallow, M. A. Khanfar, M. Malischewski, P. Finke, M. Hesse, E. Lork, T. Augenstein, F. Breher, J. R. Harmer, N. V. Vasileva, A. Zibarev, A. S. Bogomyakov, K. Seppelt, J. Beckmann, *Chem. Sci.* **2015**, *6*, 497–504.
[22] In one failed attempt, the dechalcogenation of $(2,6\text{-}Mes_2C_6H_3E)_2$ (E = S, Se, Te) using copper powder was tried. In another failed attempt we prepared 2,6-$Mes_2C_6H_3SCl$ and 2,6-$Mes_2C_6H_3SeCl$, which were fully characterized (see the Supporting Information). However, no reaction of the latter with 2,6-$Mes_2C_6H_3Li$ was observed.
[23] From the decomposition products, a small crop of colorless crystals of 2,6-$Mes_2C_6H_3Se(O)OH$ was isolated which, was characterized by an X-Ray diffraction experiment (see the Supporting Information).
[24] J. Oddershede, L. Henriksen, S. Larsen, *Org. Biomol. Chem.* **2003**, *1*, 1053–1060.
[25] T. M. Klapötke, B. Krumm, M. Scherr, *Inorg. Chem.* **2008**, *47*, 4712–4722.
[26] Y. Okada, M. Oba, A. Arai, K. Tanaka, K. Nishiyama, W. Ando, *Inorg. Chem.* **2010**, *49*, 383–385.
[27] Deposition Number(s) 2215859 (**1 a**), 2215860 (**1 b**), 2215861 (**1 c**), 2215862 [**1 c**][$B(C_6F_5)_4$], 2215863 (**2**), 2215864 (**3**) and 2215865 (**4**) contain(s) the supplementary crystallographic data for this paper. These data are provided free of charge by the joint Cambridge Crystallographic Data Centre and Fachinformationszentrum Karlsruhe Access Structures service.

[28] S. Grilli, L. Lunazzi, A. Mattanti, *J. Org. Chem.* **2001**, *66*, 4444–4446.
[29] J. Kahr, C. Moser, S. Spirk, F Belaj, R. Pietschnig, *Phosphorus Sulfur Silicon Relat. Elem.* **2014**, *189*, 1467–1474.
[30] T. M. Klapötke, B. Krumm, P. Mayer, K. Polborn, I. Schwab, *Z. Anorg. Allg. Chem.* **2005**, *631*, 2677–2682.
[31] a) J. Beckmann, M. Hesse, H. Poleschner, K. Seppelt, *Angew. Chem. Int. Ed. Engl.* **2007**, *46*, 8277–8280.
[32] H. Poleschner, S. Ellrodt, M. Malischewski, J. Nakatsuji, C. Rohner, K. Seppelt, *Angew. Chem. Int. Ed. Engl.* **2012**, *51*, 419–422.
[33] Unfortunately, 2,6-$Mes_2C_6H_3SF_3$ and 2,6-$Mes_2C_6H_3SeF_3$ could not be obtained by either of these ways.
[34] The characterization of **2**–**4** benefits from the indicative NMR nuclei. The mixed valent *m*-terphenyl tellurenyl fluoride (2,6-$Mes_2C_6H_3$)F_2TeTe(2,6-$Mes_2C_6H_3$) (**2**) has ^{125}Te chemical shifts (CD_2Cl_2) at $\delta = 1519.17$ and 1210.78 ppm, which split up as a triplet of doublets with a coupling constant of $^1J(^{125}Te\text{-}^{19}F) = 1130.48$ Hz and $^1J(^{125}Te\text{-}^{125}Te) = 12.14$ Hz and a triplet with a coupling constant of $^2J(^{125}Te\text{-}^{19}F) = 74.46$ Hz. The ^{19}F NMR spectrum (CD_2Cl_2) of **2** shows a singlet at $\delta = -95.01$ ppm. The ^{125}Te NMR spectrum (CD_2Cl_2) of 2,6-$Mes_2C_6H_3TeF_3$ (**3**) shows a doublet of triplet at $\delta = 1635.7$ ppm and coupling constants of $^1J(^{125}Te\text{-}^{19}F) = 2286$ and 314 Hz. The ^{19}F NMR spectrum (CD_2Cl_2) of **3** shows two signals in an integral ratio of 2:1, a doublet at $\delta = -59.23$ ppm and a triplet at $\delta = -125.25$ ppm both providing a coupling constant of $^3J(^{19}F\text{-}^{19}F) = 31.1$ Hz. The ^{125}Te NMR spectrum (CD_2Cl_2) of **4** shows a triplet at $\delta = 1289.22$ ppm with a $^1J(^{125}Te\text{-}^{19}F)$ coupling of 313.6 Hz. The ^{19}F NMR spectrum ($CDCl_3$) shows a singlet at $\delta = -103.13$ ppm.
[35] T. M. Klapötke, B. Krumm, P. Mayer, K. Polborn, I. Schwab, *Z. Anorg. Allg. Chem.* **2005**, *631*, 2677–2682.
[36] Surprisingly, no reaction occurred between **4** and other more conventional reducing agents, such as $LiAlH_4$, $NaBH_4$, Na_2S, BH_3-THF, magnesium and zinc. Sodium and potassium led to decomposition.
[37] K. Seppelt, D. Lentz, G. Klöter, *Inorg. Synth.* **1986**, *24*, 27–31.
[38] D. Lentz, H. Pritzkow, K. Seppelt, *Inorg. Chem.* **1978**, *17*, 1926–1931.
[39] In separate experiments, the reaction of one or two equivalents of 2,6-$Mes_2C_6H_3Li$ with pure $S(O)F_2$ exclusively provided 2,6-$Mes_2C_6H_3S(O)F$ and $(2,6\text{-}Mes_2C_6H_3)_2SO$, respectively, which were isolated as colorless crystals and fully characterized (see the Supporting Information). All attempts to reduce the sulfoxide $(2,6\text{-}Mes_2C_6H_3)_2SO$ with reducing agents, such $LiAlH_4$, $NaBH_4$, $BH_3 \cdot SMe_2$ or Na_2S, gave no reaction, whereas harsher conditions involving alkaline metals lead to decomposition.
[40] In order to synthesize $(2,6\text{-}Mes_2C_6H_3)_2SO$ in a rational way also 2,6-$Mes_2C_6H_3S(O)Cl$ and 2,6-$Mes_2C_6H_3S(O)OMe$ were synthesized and fully characterized (see the Supporting Information). Following reactions with 2,6-$Mes_2C_6H_3Li$ showed no reaction at all.
[41] P. Komorr, M. Olaru, E. Hupf, S. Mebs, J. Beckmann, *Chem. Eur. J.* **2022**, *28*, e202201023.
[42] Unfortunately, the analogous reaction with the more labile selenium complex $IPrSeF_2$ and 2,6-$Mes_2C_6H_3Li$ did not work in the same way.
[43] Half-wave potentials were quoted with reference to a saturated calomel electrode (SCE). For detailed information on CV studies, determination of $E_{1/2}$ potentials and the number of electrons transferred, see the Supporting Information.
[44] For single-electron oxidations with XeF_2 in the presence of fluoride acceptors, see: H. Poleschner, K. Seppelt, *Angew. Chem. Int. Ed. Engl.* **2013**, *52*, 12838–12842.
[45] M. Björgvinsson, T. Heinze, H. W. Roesky, F. Pauer, D. Stalke, G. M. Sheldrick, *Angew. Chem. Int. Ed. Engl.* **1991**, *30*, 1677–1678.
[46] R. W. F. Bader, *Atoms in Molecules. A Quantum Theory*; Cambridge University Press: Oxford U. K., **1991**.
[47] M. Kohout, *Int. J. Quantum Chem.* **2004**, *97*, 651–658.
[48] E. R. Johnson, S. Keinan, P. Mori-Sanchez, J. Contreras-García, A. J. Cohen, W. Yang, *J. Am. Chem. Soc.* **2010**, *132*, 6498–6506.
[49] The results for the S and Se analogues are given in the Supporting Information (see Figures S53–S55).
[50] D. Duvinage, L. A. Malaspina, S. Grabowksy, S. Mebs, J. Beckmann, *Eur. J. Inorg. Chem.* **2022**, e202200482.
[51] M. Olaru, D. Duvinage, E. Lork, S. Mebs, J. Beckmann, *Angew. Chem. Int. Ed. Engl.* **2018**, *57*, 10080–10084.
[52] Z. Li, W. Liu, *J. Chem. Theory Comput.* **2016**, *12*, 238–260.
[53] C. Cremer, M. Goswami, C. K. Rank, B. de Bruin, F. W. Patureau, *Angew. Chem. Int. Ed. Engl.* **2021**, *60*, 6451–6456.

Manuscript received: November 10, 2022
Accepted manuscript online: November 23, 2022
Version of record online: January 10, 2023